

Evidence for Charge Delocalization in Diazafluorene Ligands Supporting Low-Valent [Cp*Rh] Complexes

Wade C. Henke,^a Jonah P. Stiel,^a Victor W. Day,^a and James D. Blakemore^{*,a}

[a] W.C. Henke, J.P. Stiel, Dr. V.W. Day, Prof. J.D. Blakemore
Department of Chemistry
University of Kansas
1567 Irving Hill Road, Lawrence, Kansas 66045, United States
E-mail: blakemore@ku.edu; Tel: +1 (785) 864-3019

Abstract: Ligands based upon the 4,5-diazafluorene core are an important class of emerging ligands in organometallic chemistry, but the structure and electronic properties of these ligands have received less attention than they deserve. Here, we show that 9,9'-dimethyl-4,5-diazafluorene (Me₂daf) can stabilize low-valent complexes through charge delocalization into its conjugated π -system. Using a new platform of [Cp*Rh] complexes with three accessible formal oxidation states (+III, +II, and +I), we show that the methylation in Me₂daf is protective, blocking Brønsted acid-base chemistry commonly encountered with other daf-based ligands. Electronic absorption spectroscopy and single-crystal X-ray diffraction analysis of a family of eleven new compounds, including the unusual Cp*Rh(Me₂daf), reveal features consistent with charge delocalization driven by π -backbonding into the LUMO of Me₂daf, reminiscent of behavior displayed by the workhorse 2,2'-bipyridyl ligand. Taken together with spectrochemical data demonstrating clean conversion between oxidation states, our findings show that 9,9'-dialkylated daf-type ligands are promising building blocks for applications in reductive chemistry and catalysis.

Introduction

Development of systems that can carry out difficult reduction reactions, like conversion of CO₂ and N₂ into fuels and chemicals, is an important goal of redox chemistry.^[1,2] Redox non-innocent ligands can directly assist in these reaction sequences with redox load management.^[3,4] Consequently, development of redox non-innocent and/or redox-active ligands is an active area, particularly due to the need for stability across oxidation states and under highly reducing conditions.^[5]

One family of ligands that is well known for use in both redox and photoredox catalytic applications includes 2,2'-bipyridyl and its derivatives.^[6] 2,2'-bipyridyl (bpy) was prepared very early by Blau,^[7] but has since become one of the most popular supporting ligands in inorganic and organometallic chemistry.^[8] Some features that enable 2,2'-bipyridyl to support catalysts include: (i) the presence of two nitrogen donor atoms that can bond effectively with most transition metals by forming a stable five-membered metallacycle, (ii) the presence of a conjugated 12 π -electron system that can stabilize electron-rich intermediates through π -backbonding and charge delocalization, and (iii) a chemically robust structure lacking Brønsted-acidic or reactive moieties that could engage in deleterious side reactions. Widespread use of bpy has promoted significant creative work in the development of ligands that are adept at stabilizing metal complexes, but with tuneable properties.^[6]

By comparison, 4,5-diazafluorene (daf) is a much newer ligand technology, with the first synthesis being reported in 1950 by Schmidt and co-workers.^[9] The structures of daf-based ligands are reminiscent of bpy, but they are distinguished by the presence of an additional sp^3 hybridized carbon atom that ties the two pyridyl rings together; this establishes an additional five-membered carbocycle, rigidifying the daf core (see Chart 1). The presence of this additional five-membered ring also “pulls back” the nitrogen donor atoms, increasing the bite angle.^[10] Thus, unlike bpy, which typically and reliably binds transition metals in an $[N,N]$ -bidentate (κ^2) fashion, daf-type ligands have demonstrated the ability to coordinate metals in pentahapto (η^5),^[11] bridging (μ),^[12,13] and monodentate (κ^1)^[14] modes, as well as the more familiar κ^2 mode.

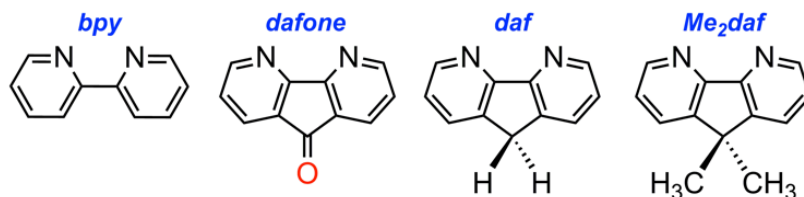


Chart 1: The structures of 2,2'-bipyridyl (bpy), 4,5-diazafluoren-9-one (dafone), 4,5-diazafluorene (daf), and 9,9'-dimethyl-4,5-diazafluorene (Me₂daf).

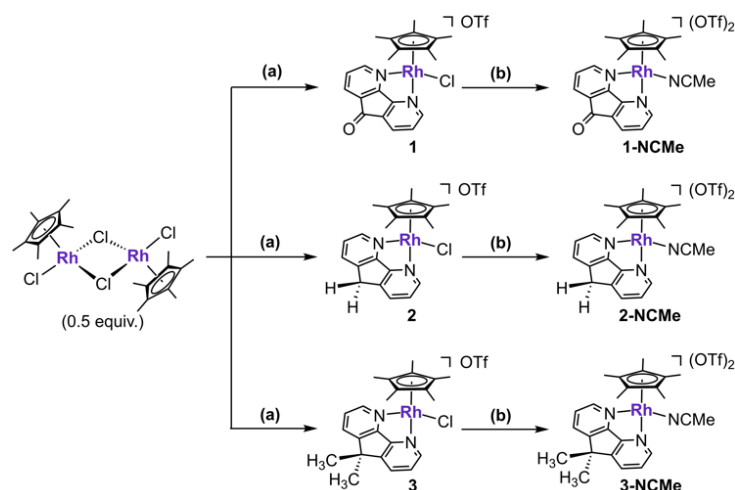
On the other hand, the structure of daf features Brønsted-acidic, doubly benzylic C–H bonds on the backbone of the ligand that can become directly involved in reactivity. For reference, cyclopentadiene, fluorene, and pentamethylcyclopentadiene have pK_a 's of 18.0, 22.6, and 26.1 in dimethyl sulfoxide; the acidity of fluorene is consistent with the behavior of daf toward deprotonation in the presence of metals.^[15] Indeed, Song and co-workers^[16,17] have leveraged daf for use in heterolytic dihydrogen splitting^[18] and olefin hydrogenation^[19]. Complementing this work, Stahl and co-workers have recently shown that congeners of daf, especially 4,5-diazafluoren-9-one (dafone) and 9,9'-dimethyldiazafluorene (Me₂daf) impart significant advantages in Pd-catalyzed acetoxylation,^[20] dehydrogenation,^[21] and aerobic oxidation reactions.^[14]

In view of these promising uses of daf-type ligands in redox chemistry and catalysis, we were surprised to find that little spectroscopic or structural evidence is available regarding the ability of the daf framework to delocalize electron density or form reduced species by charge transfer events. The latter behavior underpins the exemplary performance of $[Ru(bpy)_3]^{2+}$ in catalysis, wherein direct electron transfer or light-promoted metal-to-ligand charge transfer events drive important reactivity. The photochemically accessible states are not unlike bpy-centered radicals, in that the reducing electron density resides on the conjugated bpy framework.^[22,23] In the former case, delocalization of electron density into the bpy framework occurs via π -backdonation from low-valent, reducing metal centers, for example in $Cp^*Rh(bpy)$ (where Cp^* is pentamethylcyclopentadienyl).^[24,25,26,27] In this situation, the formally Rh(I) center donates electron density into the lowest unoccupied molecular orbital (LUMO) of bpy, stabilizing the compound. This is observed in the solid-state structure of the reduced $Cp^*Rh(bpy)$, where the C–C bond interconnecting the two pyridyl rings is noticeably shorter in comparison to that in Rh(III) analogues, confirming π -backdonation into bpy.^[28] Hoping to investigate the possibility that daf-based ligands could exhibit similar behaviors, we anticipated that the demonstrated Brønsted acid-base reactivity of daf would likely muddle studies of charge delocalization into the conjugated ligand framework. In such a scheme, we imagined that protective methylation of the 9 and 9' positions could allow such studies by disfavoring acid-base reactivity, unlocking the ability to study reduced forms of the diazafluorene core.

Here, we report the synthesis, structural characterization, and electrochemical studies of a series of [Cp*Rh] complexes supported by dafone, daf, and Me₂daf. We find that the complexes bearing dafone and daf undergo reduction-induced chemical reactivity via pathways that are arrested when using Me₂daf; methylation of daf prevents the harmful ligand-driven radical chemistry and undesired Brønsted acid/base reactivity observed in other congeners. Use of Me₂daf affords access to distinctive rhodium species in the formal +III, +II, and +I oxidation states and enables spectroscopic characterization, demonstrating that Me₂daf actively stabilizes the reduced species. Single-crystal X-ray diffraction analysis of Cp*Rh(Me₂daf) reveals the structural changes associated with delocalization of electron density into the Me₂daf framework for the first time. Our quantitative data show that the more constrained binding geometry of Me₂daf moderates its σ -donor and π -acceptor properties relative to bpy. Taken together, this study shows that Me₂daf is a promising supporting ligand for the development of redox chemistries and encourage utilization of the daf framework under reducing conditions.

Results and Discussion

Diazafluorene-type ligands^[9,29,30,31] have not previously been used for preparation of [Cp*Rh] complexes. Based on the similarity of the daf framework to bpy, we selected synthetic procedures that have previously been useful for preparation of [Cp*Rh] complexes supported by bpy and other bidentate ligands.^[32,33] We find that [Cp*RhCl₂]₂ is readily cleaved by dafone, daf, and Me₂daf,^[34,35] enabling us to access the new complexes [Cp*RhCl(dafone)]OTf, [Cp*RhCl(daf)]OTf, and [Cp*RhCl(Me₂daf)]OTf (**1-3**, see Scheme 1). Cleavage of [Cp*RhCl₂]₂ was facilitated here through use of salt metathesis with AgOTf, favoring binding of the daf-based ligands. No unusual behaviors were encountered in these syntheses, and following generation of the desired complexes, they were fully characterized (see SI, Figures S1-S9, S27-S29, and S31-S36).



Scheme 1: Synthesis of **1**, **2**, **3**, **1-NCMe**, **2-NCMe**, and **3-NCMe**. (a) 1. AgOTf (1 equiv.) in MeCN; 2. Appropriate daf-based ligand (1 equiv.) in MeCN, (b) AgOTf (1 equiv.) in MeCN.

Nuclear magnetic resonance (NMR) spectroscopic studies revealed that **1**, **2**, and **3** each exhibit C_s symmetry in solution, consistent with κ^2 -[*N,N*]-coordination of the bidentate ligands and free rotation of

[η^5 -Cp*]. The spectrum of **2** features a singlet at 4.32 ppm (integrating to 2H), which corresponds to the diastereotopic methylene protons in the daf backbone; the appearance of a singlet for these chemically inequivalent protons is attributable to coincidental magnetic equivalence of the two individual methylene protons. $^1\text{H-NMR}$ of **3** confirmed the presence of two diastereotopic methyl groups (both chemically and magnetically inequivalent) appearing as unique singlets that each integrate to 3H at 1.67 and 1.55 ppm. Taken together, these results confirm the expected connectivity of **1**, **2**, and **3** in solution.

In order to enable comprehensive electrochemical work (*vide infra*), acetonitrile-bound complexes **1-NCMe**, **2-NCMe**, and **3-NCMe** were also prepared by addition of 1 equiv. of AgOTf to **1**, **2**, and **3** (see Scheme 1 and Experimental Section for details). $^1\text{H-NMR}$ spectra confirmed clean generation of the desired solvento species in all cases (see SI, Figures S10-S17). Contrasting with results for **2**, the $^1\text{H-NMR}$ spectrum of **2-NCMe** features a pair of doublets corresponding to the chemically and magnetically inequivalent diastereotopic methylene protons of the daf backbone. The resonances are reminiscent of those corresponding to the diastereotopic methylene protons of related daf complexes.^[36] To confirm our assignment of these resonances, we carried out multifrequency NMR experiments at 400, 500, 600, and 800 MHz that confirm the involvement of second-order effects which are visible in the spectra as “roofing”. Digital simulations of the field-dependent spectra reproduced the experimental data, confirming our assignment (see SI, Figure S26).

Table 1: Selected bond lengths and angles in complexes **1**, **2**, **3**, **bpy**^{Cl}, **1-NCMe**, **2-NCMe**, **3-NCMe**, and **bpy**^{NCMe}.

Compound	Rh–N1 (Å)	Rh–N2 (Å)	Rh–L (Å)	d _{c-c} ^b (Å)	Rh–Cp* _{cent} (Å)	∠ N–Rh–N	∠ Cp* _{cent} –Rh–N* ^c	Reference
1 ^a	2.202(3), 2.197(3)	2.199(3), 2.197(3)	2.399(1), 2.402(1)	1.445(5), 1.438(5)	1.765, 1.764	80.4(1) [°] , 80.2(1) [°]	150.9 [°] , 151.5 [°]	<i>This Work</i>
2	2.185(4)	2.183(4)	2.384(1)	1.422(7)	1.770	80.1(1) [°]	148.0 [°]	<i>This Work</i>
3	2.202(4)	2.184(4)	2.392(1)	1.424(7)	1.776	80.3(2) [°]	146.0 [°]	<i>This Work</i>
bpy ^{Cl}	2.140(7)	2.140(7)	2.379(3)	1.490(17)	1.774	75.3(4) [°]	147.7 [°]	38
1-NCMe	2.200(3)	2.191(2)	2.098(3)	1.441(4)	1.774	80.28(9) [°]	147.0 [°]	<i>This Work</i>
2-NCMe ^a	2.174(3), 2.184(3)	2.225(3), 2.171(3)	2.101(3), 2.088(3)	1.428(8), 1.416(6)	1.775, 1.778	80.2(1) [°] , 81.8(2) [°]	149.9 [°] , 149.2 [°]	<i>This Work</i>
3-NCMe ^a	2.190(6), 2.204(6)	2.188(7), 2.191(6)	2.102(7), 2.088(7)	1.434(11), 1.445(10)	1.768, 1.767	81.2(2) [°] , 80.6(2) [°]	150.9 [°] , 147.2 [°]	<i>This Work</i>
bpy ^{NCMe} ^a	2.097(2), 2.109(2)	2.104(2), 2.112(2)	2.074(2), 2.066(2)	1.467(3), 1.466(3)	1.780, 1.783	77.09(6) [°] , 76.74(7) [°]	146.1 [°] , 148.0 [°]	39

^aValues for the independent molecules in the asymmetric unit cell are listed. ^bRefers to the bond between the two central carbons interconnecting the two pyridyl-like rings. ^cangle between the Cp* centroid, Rh center, and N1,N2 centroid.

Single crystals of **1**, **2**, **3**, **1-NCMe**, **2-NCMe**, and **3-NCMe** suitable for X-ray diffraction (XRD) analysis were obtained by vapor diffusion of diethyl ether into concentrated MeCN solutions of the appropriate complex. The resulting structures are the first examples of [Cp*Rh] complexes ligated by dafone, daf, and Me₂daf, and these structures provide a comprehensive basis for the interpretation of the structural properties of the complexes. The coordination geometries about the Rh centers are *pseudo*-

octahedral in each case, with η^5 -Cp* and κ^2 -[N,N]-daf-type ligands present in addition to bound chloride (**1**, **2**, and **3**) or acetonitrile (**1-NCMe**, **2-NCMe**, and **3-NCMe**) (see Table 1, Figure 1, and SI, pp. S38-S52). Overall, the Rh–L (where L = Cl or MeCN) and Rh–Cp*_{cent} distances are similar across the series, consistent with the identical formal oxidation state (+III) of the rhodium centers. The angles formed between the Cp* centroids, the Rh centers, and the centroids of the two nitrogen atoms of the diimine ligands (Cp*–Rh–N*, see Table 1) lie in a narrow range of 147–151° for all of the compounds, consistent with the similar steric profiles of all three daf-type ligands studied here.^[37]

The unique geometries of the 5-membered metallacycles formed by coordination of the daf-type ligands in these complexes can be best understood by comparing the metallacycles present in the analogous structures [Cp*Rh(bpy)Cl]OTf (**bpy**^{Cl}) and [Cp*Rh(bpy)NCMe]PF₆ (**bpy**^{NCMe}).^[38,39] In particular, the N1–Rh–N2 bite angles are ca. 5° wider for **1**, **2**, and **3** compared to **bpy**^{Cl} while the N1–Rh–N2 bite angles are ca. 4° wider for **1-NCMe**, **2-NCMe**, and **3-NCMe** compared to **bpy**^{NCMe}. This is attributable to the strained geometry induced by the fused five-membered carbocycles in all of the daf-type complexes. Confirming this situation, the Rh–N1 and Rh–N2 bond lengths are longer than those in the analogous bpy complexes by ca. 0.05–0.10 Å. This suggests an attenuation of the σ -donor power of the daf-type ligands, in that the more rigid structure constrains the flexibility of the ligands upon coordination and elongates the Rh–N distances in comparison to those found in the analogous bpy species.

The presence of the fused five-membered carbocycles in all the daf-type complexes also impacts the intraligand bond distances in coordinated dafone, daf, and Me₂daf. In particular, the C–C bonds that directly link the pyridyl-like rings of the daf-type ligands are noticeably shorter than the corresponding C–C bonds in the bpy complexes. These distances, denoted as d_{C–C} with values given in Table 1, are shorter by ca. 0.07 Å and ca. 0.03 Å for **3** and **3-NCMe**, respectively, vs. their bpy analogues.

In order to understand the oxidation states accessible to [Cp*Rh] complexes with daf-type ligands, we carried out electrochemical studies. Initially, we examined the voltammetric properties of **1**, **2**, and **3**, but encountered quasireversible and irreversible reductive waves that are consistent with significant chemical reactivity upon reduction of the starting Rh(III) complexes (see SI, Figures S38, S41, and S43). In particular, the electrochemical data for **3** is consistent with generation of a Rh(II) species by initial electron transfer to the complexes, followed by loss of the daf-type ligands and formation of [Cp*RhCl]₂.^[40] Formation of [Cp*RhCl]₂ is also supported by related chemical work examining the products of reduction of **3** by Cp₂Co (see SI, Figure S25); here, the presence of [Cp*RhCl]₂ could be confirmed by i) ¹H-NMR spectra showing a singlet at 1.60 ppm and ii) visually with the appearance of a blue colored solution. Notably, we have previously encountered the generation of [Cp*RhCl]₂ in electrochemical work with chloride-bound complexes supported by dipyritylmethane (dpma) ligands.^[41,42] Complexes supported by daf-type ligands resemble those supported by dpma ligands in that both classes feature strained metallacycles that may cause bidentate ligands to be prone to decoordination from rhodium metal centers upon formation of the labile +II oxidation state in the presence of chloride. In order to avoid this complication driven by the chloride ligands, we turned our focus to the electrochemical properties of the solvento complexes.

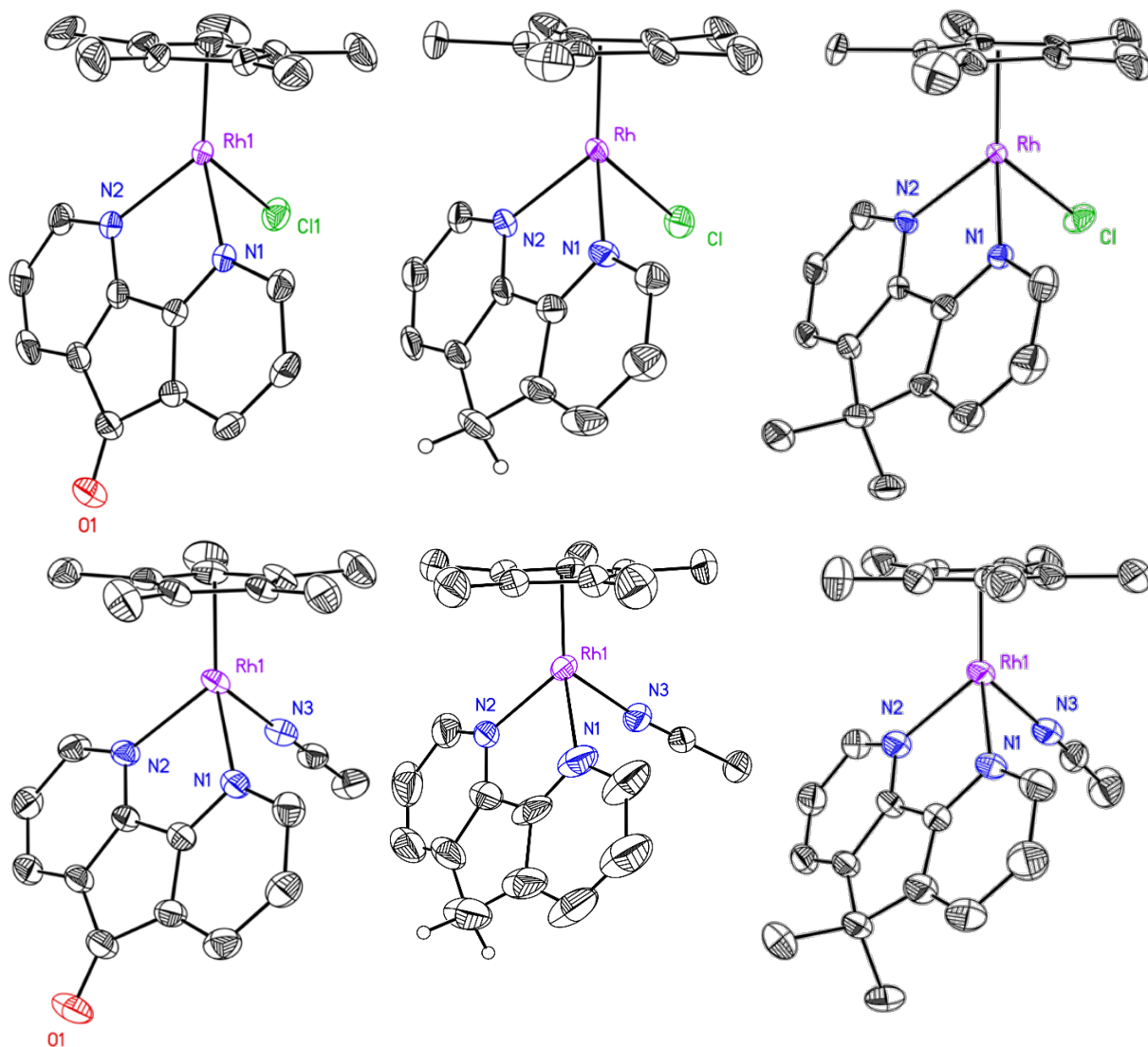


Figure 1: Solid-state structures of **1** (upper left), **1-NCMe** (lower left), **2** (upper middle), **2-NCMe** (lower middle), **3** (upper right) and **3-NCMe** (lower right). Displacement ellipsoids are shown at the 50% probability level. Hydrogen atoms (except H11A and H11B for **2** and **2-NCMe**), outer sphere triflate counteranions, any co-crystallized solvent molecules, and secondary molecular cations present in the asymmetric units of **1**, **2-NCMe**, and **3-NCMe** are omitted for clarity.

Electrochemical studies of **1-NCMe**, **2-NCMe**, and **3-NCMe** reveal the rich electrochemical properties of these systems in the absence of complications from chloride (see Figure 2, and SI, Figures S39, S42, and S44). Qualitatively, the voltammograms of all three complexes reveal two individual cathodic reduction events in each case, as well as two return anodic oxidation events. This suggests that formally Rh(III), Rh(II), and Rh(I) species are accessible with dafone, daf, and Me₂daf. However, the behavior of **1-NCMe** and **2-NCMe** can be described as quasireversible at best, considering the attenuated anodic currents associated with the re-oxidation of the products of reduction.^[43] The diminished currents for the return oxidations indicate that follow-up chemical reactivity ensues after the initial reductions and that the reduced forms thus have limited stability. The instability implied by the voltammetry is consistent, however, with the presence of the ketone moiety in dafone and the methylene group in daf. In the case of

dafone, the benzophenone-like core could undergo formation of radical species.^[44] Similarly, the doubly benzylic methylene group in daf is likely to be sufficiently acidic to undergo deprotonation by nascent Rh(I) when it is formed. Two lines of evidence support this reactivity: first, the cyclic voltammogram of **2-NCMe** features a first reduction wave that is significantly more reversible than the second (see Figure 2, middle panel and SI, Figure S42); second, chemical reduction experiments suggest that the Rh(I) form of **2-NCMe** is sufficiently basic to deprotonate the starting Rh(III) form (See SI, pp. S54-S55).^[17,45]

Contrasting with these results, the cyclic voltammogram of **3-NCMe** reveals that Me₂daf enables clean generation of both Rh(II) and Rh(I) forms of the complex under electrochemical conditions. This conclusion is supported by the chemically reversible nature of the two, sequential 1e⁻ reductions present in the voltammetry (see Figure 2, lower panel) as well as related chemical reduction experiments (*vide infra*). Studies at scan rates between 50 and 300 mV/s retain the chemical reversible appearance of the voltammetry, supporting both the stability of the reduced forms as well as the soluble, diffusional nature of all three accessible oxidation states of the compound (see SI, Figures 45-46). Thus, we conclude that use of Me₂daf in place of daf protects the Cp*Rh] complex from detrimental follow-up reactivity upon reduction.

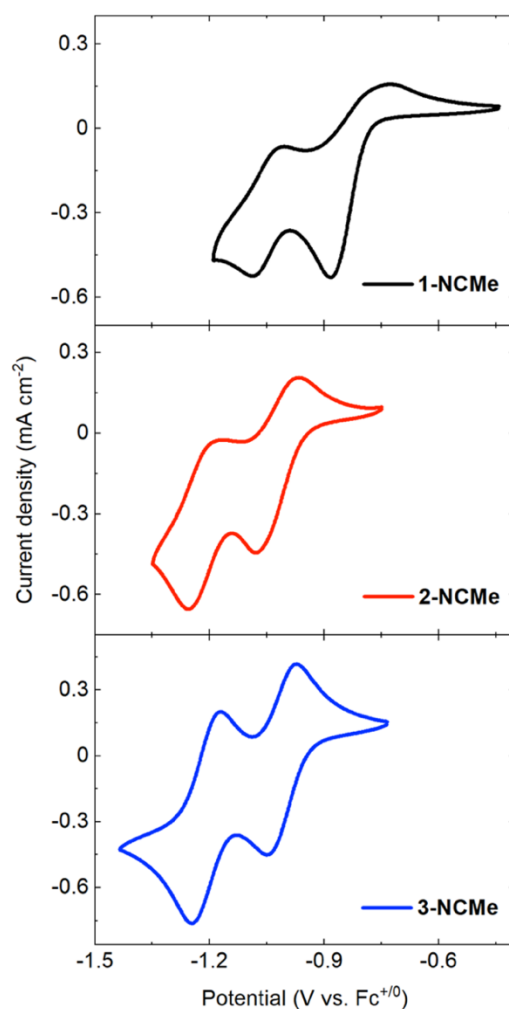


Figure 2: Cyclic voltammograms (MeCN, 0.1 M [nBu₄N][PF₆], 100 mV s⁻¹) of **1-NCMe** (upper panel), **2-NCMe** (middle panel), and **3-NCMe** (lower panel).

Returning to the question of the role of chloride in these complexes, we carried out an electrochemical titration of **3-NCMe** with chloride (in the form of NBu_4Cl) in order to track the generation of **3** upon chloride binding. The findings of this titration (see SI, Figure S48) confirm that chloride contributes to the irreversible behavior encountered in electrochemical studies of **3**. In light of these experiments, **3** can be assigned to undergo a single, net $2e^-$ reduction event in contrast to the two sequential $1e^-$ events measured for **3-NCMe**. This profile is reminiscent of a $[\text{Cp}^*\text{Rh}]$ complex ligated by a hybrid phosphine-imine ligand that our group has studied; this compound displays a net $2e^-$ reduction wave with a chloride ligand present, but two $1e^-$ waves when isolated as a solvento complex.^[46] Dipyridylmethane-ligated $[\text{Cp}^*\text{Rh}]$ systems also show net $2e^-$ vs. $1e^-$ chemistry when studied with or without chloride.^[42] These findings are overall consistent with the *in situ* production of **3** over the course of the chloride titration and underscore the broad importance of chloride in the redox chemistry of $[\text{Cp}^*\text{Rh}]$ complexes.

Summarizing, the electrochemical data for **3-NCMe** reveal sequential $1e^-$ reductions at -1.04 V and -1.25 V vs. the ferrocenium/ferrocene couple (denoted hereafter as $\text{Fc}^{+/0}$). Similarly, the data for **2-NCMe** reveal reductions at -1.07 V and -1.25 V. In both cases, the more positive wave can be assigned to reduction of Rh(III) to Rh(II) and the more negative wave can be assigned to reduction of Rh(II) to Rh(I). However, the chemical reversibility of **3-NCMe** appears significantly better than that of **2-NCMe**.

Based on the greater chemical reversibility of electrochemical data for **3-NCMe**, we next moved to generate the Rh(II) and Rh(I) forms of the compound by chemical reduction. We selected cobaltocene (Cp_2Co) for this work based on its reduction potential ($E_{1/2} \approx -1.34$ V vs. $\text{Fc}^{+/0}$),^[47] which we anticipated is sufficiently negative to be effective for generation of first Rh(II) and then Rh(I). We performed a spectrochemical titration by treating **3-NCMe** with substoichiometric equivalents of Cp_2Co while monitoring the solution with UV-visible absorption (UV-vis) spectroscopy. The starting spectrum of **3-NCMe** is unremarkable and similar to other Rh(III) species that we have studied,^[4,48] with an absorption centered at 373 nm (see Figure 3 and see SI, Figures S49-S52). Upon addition of Cp_2Co up to 1 equiv. per Rh, the spectrum changes substantially, with the most obvious difference being the growth of a new band at 716 nm, which corresponds to the Rh^{II} form of **3**. We observe clean $1e^-$ reduction of **3-NCMe** with isosbestic points at 223, 246, 320, and 349 nm. As the initial concentration of **3-NCMe** and the various concentrations of Cp_2Co were known, we determined the molar absorptivity of the new band at 716 nm to be $3200 \text{ M}^{-1} \text{ cm}^{-1}$ (see SI, Figure S49).

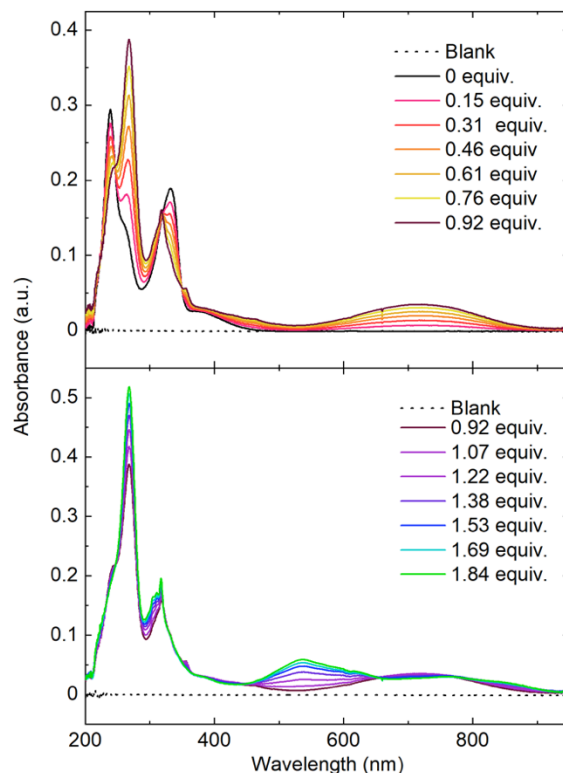


Figure 3: Spectrochemical titration of **3-NCMe** using Cp_2Co as a reductant in THF solution. Upper panel: data corresponding to generation of Rh^{II} . Lower panel: data corresponding to generation of Rh^{I} .

Continued additions of Cp_2Co up to 2 equiv. per 1 equiv. of **3-NCMe** resulted in growth of a new feature at 534 nm, as well as sharpening of both shorter and longer wavelength absorption features to reveal apparent vibronic coupling. Vibronic bands were observed at 305, 310, and 317 nm in the UV region, similar to bands at 316, 324, and 332 that we observed for the $[\text{Mn}^{\text{I}}(\text{CO})_3]$ complex of Me_2daf .^[36] Longer wavelength vibronic bands were also observable at 697, 763, and 835 nm. Isosbestic points at 247, 320, and 660 nm in this data are consistent with clean generation of the Rh^{I} form of **3**, namely $\text{Cp}^*\text{Rh}(\text{Me}_2\text{daf})$ (**4**, *vide infra*). This species represents a notable analogue of $\text{Cp}^*\text{Rh}(\text{bpy})$, which features a very similar UV-visible absorption spectrum; $\text{Cp}^*\text{Rh}(\text{bpy})$ displays an absorption at 515 nm as well as longer wavelength features with absorption maxima at ca. 684, 749, and 824 nm (see SI, Figure S37).

Delocalization of electron density from $\text{Rh}(\text{I})$ into the bpy ligand in $\text{Cp}^*\text{Rh}(\text{bpy})$ has been discussed in a significant body of prior work; this phenomenon gives rise to the long wavelength absorptions and apparent vibronic features, which are derived from intra- bpy vibrations.^[22] Considering the striking similarity between the spectral profiles of $\text{Cp}^*\text{Rh}(\text{bpy})$ and $\text{Cp}^*\text{Rh}(\text{Me}_2\text{daf})$ (see SI, Figure S37), significant charge delocalization from the electron-rich rhodium center into the Me_2daf ligand is implicated in the data. In particular, the long wavelength absorptions displaying vibronic coupling likely arise due to intra- Me_2daf vibrations that are not unlike those present in bpy , considering the similar conjugated frameworks of these ligands. Thus, in both these cases, the long wavelength absorption bands are attributable to excitation of electron density present in the ligand π -system into higher-lying ligand π^* orbitals. The electron density in question, however, is originally derived from the formally $\text{Rh}(\text{I})$ center and is shared via backbonding.

A quantitative comparison of the molar absorptivity values for the [Cp*Rh^I] complexes of bpy and Me₂daf provides insight into their properties as ligands. The molar absorptivity values for Cp*Rh(Me₂daf) were found to be 6,200 M⁻¹ cm⁻¹ at $\lambda_{\text{max}} = 534$ nm and 3,100 M⁻¹ cm⁻¹ at $\lambda_{\text{max}} = 763$ nm. Cp*Rh(bpy), on the other hand, has corresponding molar absorptivity values of 14,900 M⁻¹ cm⁻¹ at $\lambda_{\text{max}} = 515$ nm and 4,400 M⁻¹ cm⁻¹ at $\lambda_{\text{max}} = 749$ nm. The more modest values for the Me₂daf complex can be attributed to more moderate delocalization of electron density from the formally Rh(I) center in Cp*Rh(Me₂daf) into the Me₂daf framework. The decreased population of the Me₂daf-centered π^* orbitals would lead to diminished intensities for these longer wavelength features in the absorption spectrum. These findings suggest that Me₂daf is a weaker π -acceptor than bpy, and provide evidence for similar charge delocalization behaviors for both bpy and its less commonly studied analogue Me₂daf. Confirming this theory, the Rh^{III}/Rh^I reduction potential of **3** is -1.25 V, approximately, while the value for Cp*Rh(bpy) is -1.05 V.^[49]

Characterization of the Rh^{II} form of **3-NCMe** by X-band electron paramagnetic resonance spectroscopy confirms the redox scheme described above. An *in situ* reduction experiment was carried out in which **3-NCMe** was treated with 1.0 equiv. of Cp₂Co in THF, resulting in a color change from yellow to green. The green solution was then loaded into a quartz EPR tube and frozen in liquid nitrogen for transport to the spectrometer. EPR at 7 K revealed a broad rhombic signal near $g = 2$ (see SI, Figure S53) that lacks signals corresponding to Cp₂Co.^[48] The EPR spectrum for the *in situ* reduced sample of **3-NCMe** could be satisfactorily modelled as a two-component mixture with the EasySpin simulation package.^[50] The two components, labelled as **A** and **B** are present in an apparent ratio of 2:1, both display rhombic signals (**A**: $g_x = 2.15$, $g_y = 2.03$, $g_z = 1.94$; **B**: $g_x = 2.08$, $g_y = 2.02$, $g_z = 2.00$). These overlapping signals are consistent with Rh^{II} radicals in both cases, resembling prior EPR spectra that we have obtained for [Cp*Rh^{II}] complexes. We anticipate that **A** and **B** correspond to the MeCN-bound (19e⁻) and MeCN-free (17e⁻) species, consistent with observations from prior work.^[41,42]

Consistent with these findings, reduction of **3-NCMe** with Na(Hg) enables isolation of solid Cp*Rh(Me₂daf) (**4**; see Experimental Section). Like its counterpart Cp*Rh(bpy), **4** is intensely colored and appears purple in THF solution. However, unlike Cp*Rh(bpy), **4** could only be isolated from this synthetic procedure with minor aromatic and aliphatic impurities (see SI, Figure S18-S20). Despite these slight impurities, ¹H NMR reveals that **4** exhibits C_{2v} symmetry in solution, including two singlets in the aliphatic region at 2.00 and 1.16 ppm that integrate to 15H and 6H, respectively, and correspond to the 15 equivalent methyl protons of the Cp* ligand and 6 equivalent methyl protons of the κ^2 -Me₂daf ligand. The magnetic equivalence of the methyl protons of Me₂daf in **4** suggests that this compound adopts a “T-shaped” geometry.

Single-crystal X-ray diffraction (XRD) analysis confirmed this expectation. Crystals suitable for XRD analysis were grown from a hexane solution of **4** cooled to -35 °C. The solid-state structure (see Figure 4) reveals that **4** is rigorously C_{2v} symmetric, featuring the expected η^5 -Cp* and κ^2 -Me₂daf ligands around the metal center. **4** is much more electron-rich than **3-NCMe**, as observed by the elongated Rh-Cp*_{cent} distance (1.829 Å in **4** vs. 1.768 Å in **3-NCMe**; see Tables 1 and 2). Consistent with the greater electron-richness of the metal center, the Rh-N distances are shorter in **4** compared to those in **3-NCMe** by approximately 0.13 Å, a finding that supports a role for π -backbonding into the Me₂daf ligand of this complex.

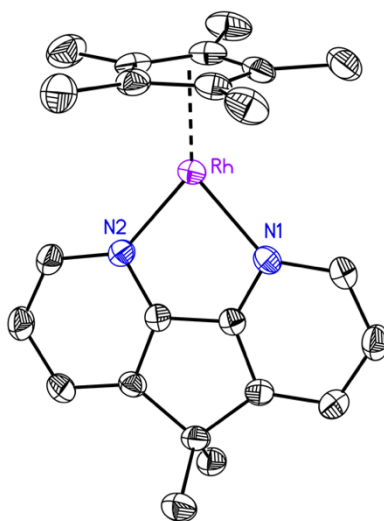


Figure 4: Solid-state structure of **4**. Displacement ellipsoids are shown at the 50% probability level. Hydrogen atoms are omitted for clarity.

Table 2: Selected bond lengths and angles in complexes **4**, Cp*Rh(bpy), and CpRh(bpy).

Bond Metrics	4	Cp*Rh(bpy)	CpRh(bpy)
Rh–N1 (Å)	2.064(2)	2.00(3)	1.993(2)
Rh–N2 (Å)	2.064(2)	2.005(2)	1.990(3)
d _{C–C} ^a (Å)	1.393(3)	1.422(4)	1.441(3)
Rh–Cp* _{cent} (Å)	1.829	1.847	1.868 ^b
∠ N–Rh–N	82.03(8) ^o	78.2(1) ^o	78.76(8) ^o
∠ Cp*–Rh–N ^c	176.4 ^o	177.3 ^o	177.1 ^o

^aRefers to the bond between the two central carbons interconnecting the two pyridyl-like rings. ^bNote, this is cyclopentadienyl (Cp) and not Cp*. ^cangle between the Cp* or Cp, centroid, Rh center, and N1,N2 centroid.

Examination of the intraligand C–C bonds of the Me₂daf ligand in **4** provides evidence for charge delocalization. This conclusion can be drawn on the basis of similar prior findings for bpy-based ligands, in that both Cp*Rh(bpy)^[38] and CpRh(bpy) (where Cp is cyclopentadienyl)^[51] display partially reduced ligand character that can be inferred from changes in their intraligand C–C bonds. Table 2 provides selected bond lengths and angles, and Figure 5 provides a full comparison of the intraligand bond lengths in the diimine ligands in these complexes. In particular, reduced bpy character has been shown to result in a pronounced contraction of the C–C bond that links the two pyridyl rings of bpy (denoted here as d_{C–C}), a phenomenon attributable to occupation of the lowest-energy unoccupied π* orbital of bpy.^[28] Occupation of the bpy LUMO contributes to the double bond character observed for d_{C–C} and can be visualized with a combination of Hückel MO theory and solid-state structural data (see Table 2).^[52] As the conjugated frameworks of Me₂daf and bpy are similar, Me₂daf can be seen on the basis of the structural data in Figure 5 to also be capable of stabilizing electron-rich Rh(I) centers via charge delocalization. **4**

displays a marked contraction of the d_{C-C} bond (1.393(3) Å) in comparison to that in **3-NCMe** (1.434(1)/1.445(10) Å), providing structural evidence that Me₂daf is able to stabilize low-valent metal centers via bonding motifs similar to those found in complexes supported by workhorse bipyridyl-type ligands. Notably, the value of d_{C-C} is significantly shorter in **4** than in its bipyridyl analogues (see Table 2 and Figure 5); this is attributable to the simultaneous influence of π -backbonding from the electron-rich metal as well as the presence of the additional five-membered fused carbocycle resulting from inclusion of the dimethylmethylene group of Me₂daf.

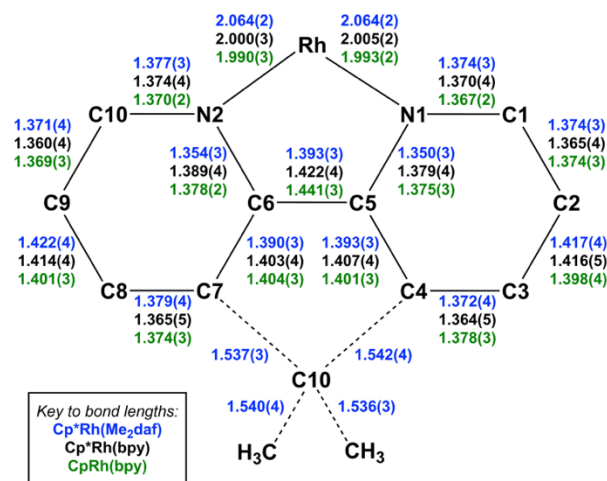


Figure 5: Comparison of intraligand bond lengths for Cp*Rh(Me₂daf) (**4**, blue), Cp*Rh(bpy) (black), and CpRh(bpy) (green).

Considering the established structural and electronic similarities between Me₂daf and bpy, we wondered if a monohydride complex or $[\eta^4\text{-Cp}^*\text{H}]$ -bound species would be preferred for the case of the Me₂daf system. Addition of weak acids to Cp*Rh(bpy) has recently been shown to result in generation of $[\eta^4\text{-Cp}^*\text{H}]$ -bound complexes rather than the expected analogous rhodium monohydrides.^[49, 53, 54] To test this, **3** was exposed to 1.0 equiv. of sodium formate in *d*₃-MeCN, resulting in a gradual color change from orange to red-brown. ¹H NMR revealed a spectrum consistent with the generation of $[(\eta^4\text{-Cp}^*\text{H})\text{Rh}(\text{Me}_2\text{daf})]^+$ (see SI, Figures S21-S23), a species that displays the hallmark resonances indicating proton transfer to the $\eta^5\text{-Cp}^*$ ligand of **3**. In particular, a quartet at 2.44 ppm (1H, ⁴J_{H,H} = 6.2 Hz) and a doublet at 0.55 ppm (3H, ⁴J_{H,H} = 6.2 Hz) confirm the generation of the $\eta^4\text{-Cp}^*\text{H}$ ligand, which presumably forms through binding of formate to Rh(III), β -hydride elimination and extrusion of CO₂, and proton-hydride tautomerization.^[53] Me₂daf can thus be additionally concluded to engender similar reactivity to $[\text{Cp}^*\text{Rh}]$ complexes in comparison to those supported by bipyridyl-type ligands.

Conclusion

Here, we have described the synthesis and characterization of a new series of $[\text{Cp}^*\text{Rh}]$ complexes supported by diazafluorene-type ligands. On the basis of structural, spectroscopic, and electrochemical evidence, 9,9'-dimethyl-4,5-diazafluorene (Me₂daf) can be concluded to be able to stabilize low-valent complexes through charge delocalization and π -backbonding that is reminiscent of behavior more

commonly encountered with complexes of 2,2'-bipyridyl and its analogues. In this work, a comprehensive set of solid-state structures from X-ray diffraction analysis has been used to highlight the bond lengths and angles that distinguish diazafluorene complexes from their more common analogues. On the basis of clean electrochemical behavior for the [Cp*Rh] species supported by Me₂daf, a spectrochemical titration was carried out with Cp₂Co that revealed the unique spectroscopic signatures of Rh(III), Rh(II), and Rh(I) supported by Me₂daf. The charge delocalization implied by the spectroscopic results for Cp*Rh(Me₂daf) was confirmed by related X-ray diffraction analysis for this compound, which showed changes in the intra-Me₂daf framework consistent with sharing of electron density from the [Cp*Rh^I] core into the LUMO of Me₂daf via π -backbonding. Use of Me₂daf in place of dafone or daf avoids detrimental reactivity under highly reducing conditions and, thus, Me₂daf can be concluded to be a useful new ligand for use in reductive chemistry and electrochemistry.

Experimental Section

General considerations

All manipulations were carried out in dry N₂-filled gloveboxes (Vacuum Atmospheres Co., Hawthorne, CA, USA) or under an N₂ atmosphere using standard Schlenk techniques unless otherwise noted. All solvents were of commercial grade and dried over activated alumina using a PPT Glass Contour (Nashua, NH, USA) solvent purification system prior to use, and were stored over molecular sieves. All chemicals were obtained from major commercial suppliers and used as received after extensive drying. Rhodium chloride hydrate (Pressure Chemical Co.) and 1,10-phenanthroline (95%; Matrix Scientific) were used as received. [Cp*RhCl₂]₂,^[34,35] 4,5-diazafluorene-9-one,^[9] 4,5-diazafluorene,^[9] and 9,9'-dimethyldiazafluorene^[30] were prepared according to literature methods with minor modifications. [Cp*RhCl₂]₂, silver hexafluorophosphate (98%, Alfa Aesar), mercury, sodium, and cobaltocene were dried extensively at 1 mTorr (133.322 Pa) for 24 hours using standard Schlenk techniques before being brought into a dry N₂-filled glovebox.

Synthesis

General Procedure for the Synthesis of 1, 2, and 3: To a 20 mL scintillation vial equipped with a Teflon stir bar, 1 equiv. of [Cp*RhCl₂]₂ was dissolved in MeCN (ca. 4mL) to give a deep red suspension. To this suspension, 2 equiv. of AgOTf in MeCN (ca. 2 mL) was added, resulting in a lightening of the red solution to orange, and formation of AgCl as a precipitate. The solution was allowed to stir for 10 min. Then 2.1 equiv. of the appropriate diazafluorene-based ligand was added to the orange solution and was allowed to stir for 20 minutes. The AgCl was then filtered off and the resulting yellow solution was placed in a beaker. Next, a large excess of diethyl ether (ca. 80 mL) was added, causing precipitation of the desired product. The yellow solid was then filtered and washed with diethyl ether. The material was purified by recrystallization through vapor diffusion of diethyl ether into a concentrated solution of the compound in MeCN. The resulting red crystals were washed with diethyl ether to afford the title compound.

[(η^5 -C₅Me₅)Rh(4,5-diazafluorene-9-one)Cl](OTf) (1): Yield: 0.3073 g (63 %). ¹H NMR (500 MHz, CD₃CN): δ = 8.83 (d, 2H, ³J_{H,H} = 5.5 Hz), 8.26 (d, 2H, ³J_{H,H} = 7.5 Hz), 7.82 (dd, 2H, ³J_{H,H} = 7.5 Hz, ⁴J_{H,H} = 5.5 Hz), 1.76 ppm (s, 15H). ¹³C {¹H} NMR (126 MHz, CD₃CN): δ = 186.69, 165.23, 154.14, 135.96, 130.96, 130.85, 97.77 (d, ¹J_{C,Rh} = 9.0 Hz, Cp*), 9.60 ppm. ¹⁹F NMR (471 MHz, CD₃CN): δ = -80.19 ppm. Electronic absorption spectrum (MeCN): 247 (22000), 307 (7100), 313 (6700), 320 (8000), 382 nm (1969

M⁻¹ cm⁻¹) ESI-MS (positive) found m/z: 455.0389 (100%) (**1** – OTf), 456.0459 (6%), 457.0396 (14%), 458.0471 (1%). Anal. Calcd. for C₂₂H₂₁ClF₃N₂O₄RhS: C, 43.69; H, 3.50; N, 4.63. Found: C, 43.69; H, 3.35; N, 4.87.

Synthesis of [(η⁵-C₅Me₅)Rh(4,5-diazafluorene)Cl](OTf) (2**):** Yield: 0.3044 g (80%). ¹H NMR (500 MHz, CD₃CN): δ = 8.72 (d, 2H, ³J_{H,H} = 5.4 Hz), 8.25 (d, 2H, ³J_{H,H} = 7.7 Hz), 7.73 (dd, 2H, ³J_{H,H} = 7.7 Hz, ⁴J_{H,H} = 5.4 Hz), 4.32 (s, 2H) 1.74 ppm (s, 15H). ¹³C {¹H} NMR (126 MHz, CD₃CN): δ = 161.48, 148.79, 138.61, 137.62, 127.98, 97.14 (d, ¹J_{C,Rh} = 9.0 Hz, Cp*), 37.51, 9.52 ppm. ¹⁹F NMR (471 MHz, CD₃CN): δ = -80.19 ppm. Electronic absorption spectrum (MeCN): 242 (19000), 315 (17000), 325 (18000), 391 nm (1557 M⁻¹ cm⁻¹). ESI-MS (positive) found m/z: 441.0605 (100%) (**2** – OTf), 442.0679 (9%), 443.0600 (12%), 444.0689 (2%). Anal. Calcd. for C₂₂H₂₃ClF₃N₂O₃RhS : C, 44.72; H, 3.92; N, 4.74. Found: C, 44.77; H, 3.86; N, 4.87.

Synthesis of [(η⁵-C₅Me₅)Rh(9,9'-dimethyl-4,5-diazafluorene)Cl](OTf) (3**):** Yield: 0.6763 g (85 %). ¹H NMR(500 MHz, CD₃CN): δ = 8.68 (d, 2H, ³J_{H,H} = 5.4 Hz), 8.20 (d, 2H, ³J_{H,H} = 7.7 Hz), 7.72 (d, 2H, ³J_{H,H} = 7.7 Hz ⁴J_{H,H} = 5.4 Hz), 1.75 (s, 15H), 1.67 (s, 3H), 1.55 ppm (s, 3H). ¹³C {¹H} NMR (126 MHz, CD₃CN): δ = 159.49, 149.01, 148.05, 135.18, 128.57, 97.17 (d, ¹J_{C,Rh} = 9.1 Hz, Cp*), 51.82, 24.94, 24.44, 9.54 ppm. ¹⁹F NMR (471 MHz, CD₃CN): δ = -80.18 ppm. Electronic absorption spectrum (MeCN):241 (18000), 319 (17000), 328 (18000), 389 nm (1570 M⁻¹ cm⁻¹). ESI-MS (positive) found m/z: 469.0911 (100%) (**3** – OTf), 470.0975 (10%), 471.1101 (25%), 472.1255 (3%). Anal. Calcd. for C₂₄H₂₇ClF₃N₂O₃RhS + 0.5 H₂O: C, 45.91; H, 4.49; N, 4.46. Found: C, 45.77; H, 4.42; N, 4.63.

General Procedure for the Synthesis of 1-NCMe, 2-NCMe, and 3-NCMe: To a solution of 1 equiv. of **1**, **2** or **3** in MeCN (ca. 5 mL) was added 1.1 equiv. of AgOTf dissolved in MeCN. The 20 mL scintillation vial was then sealed, covered with aluminum foil, and allowed to stir for 48 hrs. in the dark. Following completion, the precipitated silver chloride is filtered off and the solution is pumped to dryness. The resulting solid is transferred to a frit and washed with THF (ca. 20 mL) to remove any excess AgOTf to obtain the title compound as a yellow powder.

Synthesis of [(η⁵-C₅Me₅)Rh(4,5-diazafluorene-9-one)(NCMe)](OTf) (1-NCMe**):** Yield: 0.0548 g (47%). ¹H NMR (400 MHz, CD₃CN): δ = 8.90 (dd, 2H, ³J_{H,H} = 5.6 Hz, ⁴J_{H,H} = 1.0 Hz), 8.36 (dd, 2H, ³J_{H,H} = 7.6 Hz, ⁴J_{H,H} = 1.0 Hz), 7.92 (dd, 2H, ³J_{H,H} = 7.6 Hz, ⁴J_{H,H} = 5.6 Hz), 1.96 (s, 3H), 1.79 ppm (s, 15H). ¹⁹F NMR (376 MHz, CD₃CN): δ = -80.19 ppm.

Synthesis of [(η⁵-C₅Me₅)Rh(4,5-diazafluorene)(NCMe)](OTf) (2-NCMe**):** Yield: 0.1307 g (83%). ¹H NMR (400 MHz, CD₃CN): δ = 8.77 (dd, 2H, ³J_{H,H} = 5.5 Hz, ⁴J_{H,H} = 0.9 Hz), 8.35 (dd, 2H, ³J_{H,H} = 7.7 Hz, ⁴J_{H,H} = 0.9 Hz), 7.82 (dd, 2H, ³J_{H,H} = 7.7 Hz, ⁴J_{H,H} = 5.5 Hz), 4.40 (d, 1H, ³J_{H,H} = 21.1 Hz), 4.33 (d, 1H, ³J_{H,H} = 21.1 Hz), 1.96 (s, 3H), 1.77 ppm (s, 15H). ¹³C {¹H} NMR (126 MHz, CD₃CN): δ = 162.05, 149.29, 139.23, 138.69, 128.61, 123.39, 120.84, 100.30 (d, ¹J_{C,Rh} = 8.9 Hz, Cp*), 37.89, 9.60 ppm. ¹⁹F NMR (376 MHz, CD₃CN): δ = -80.20 ppm.

Synthesis of [(η⁵-C₅Me₅)Rh(9,9'-dimethyl-4,5-diazafluorene)(NCMe)](OTf) (3-NCMe**):** Yield: 0.2475 g (66%). ¹H NMR (400 MHz, CD₃CN): δ = 8.73 ((dd, 2H, ³J_{H,H} = 5.5 Hz, ⁴J_{H,H} = 1.0 Hz), 8.30 (dd, 2H, ³J_{H,H} = 7.7 Hz, ⁴J_{H,H} = 1.0 Hz), 7.82 (dd, 2H, ³J_{H,H} = 7.7 Hz, ⁴J_{H,H} = 5.5 Hz), 1.96 (s, 3H), 1.77 (s, 15H), 1.69 (s, 3H), 1.62 (s, 3H). ¹³C {¹H} NMR (126 MHz, CD₃CN): δ = 159.54, 149.21, 148.23, 136.05, 128.94, 123.04, 120.49, 99.99 (d, ¹J_{C,Rh} = 8.9 Hz, Cp*), 52.07, 24.11, 23.92, 9.26 ppm. ¹⁹F NMR (376 MHz, CD₃CN): δ = -80.19 ppm.

Synthesis of (η^5 -C₅Me₅)Rh(9,9'-dimethyl-4,5-diazafluorene) (4): A suspension of **3-NCMe** (0.0250 g, 0.032 mmol) in THF (ca. 2 mL) was added to a 20 mL scintillation vial containing 1% Na(Hg) (0.0074 g, 0.322 mmol Na, ca. 10 equiv.). The yellow suspension slowly darkened to an intense green color, which subsided to a dark purple color over a 24 h period while stirring. The reaction mixture was filtered to remove Hg and NaOTf. THF was then removed in vacuo and the resulting solid was extracted with hexanes (ca. 10 mL), followed by diethyl ether, to obtain the title product as a dark solid. Yield 0.0112 g (80%). ¹H NMR (500 MHz, C₆D₆): δ = 8.74 (d, 2H, ³J_{H,H} = 6.1 Hz), 6.90 (d, 2H, ³J_{H,H} = 6.6 Hz), 6.60 (t, 2H, ³J_{H,H} = 6.3 Hz), 2.00 (s, 15H), 1.16 ppm (s, 6H). ¹³C{¹H} NMR (126 MHz, C₆D₆): δ = 149.65, 147.84, 145.62, 118.74, 111.15, 87.10 (d, ¹J_{C,Rh} = 7.3 Hz, Cp*), 50.86, 24.85, 10.39 ppm.

Spectroscopy and Characterization

Deuterated solvents for NMR studies were purchased from Cambridge Isotope Laboratories (Tewksbury, MA, USA); CD₃CN was dried with CaH₂ and stored over molecular sieves and C₆D₆ was dried over sodium/benzophenone. ¹H, ¹³C, and ¹⁹F spectra were collected with 400, 500, 600, or 800 MHz Bruker spectrometers. Spectra were referenced to the residual protio-solvent signal^[55] in the cases of ¹H and ¹³C. Heteronuclear NMR spectra were referenced to the appropriate external standard following the recommended scale based on ratios of absolute frequencies (Ξ).^[56] ¹⁹F NMR spectra are reported relative to CCl₃F. Chemical shifts (δ) and coupling constants (*J*) are reported in Hz. Simulations of NMR spectra were carried out using the Advanced Spin Simulation program in MestReNova (Mestrelab Research, chemistry software solutions).

Experimental mass spectrometry data was collected on a LCT Premier mass spectrometer equipped with a quadrupole, time-of-flight mass analyzer, and an electrospray ion source. Predicted mass spectrometry data was obtained from PerkinElmer Informatics' ChemDraw Professional Suite. Electronic absorption spectra were collected with an Ocean Optics Flame spectrometer equipped with a DH-Mini light source (Ocean Optics, Largo, FL, USA) using a quartz cuvette. Elemental analyses were performed by Midwest Microlab, Inc. (Indianapolis, IN). Elemental analysis could not be obtained for **1-NCMe**, **2-NCMe**, **3-NCMe**, and **4** because of their acute air sensitivity. Continuous-wave electron paramagnetic resonance spectra were collected at X-band with a Bruker EMX spectrometer using a high-sensitivity perpendicular-mode cavity (4119HS-W1). Temperature control was achieved with an Oxford ESR 900 flow-through cryostat. Simulation of continuous-wave electron paramagnetic spectra were carried out using the EasySpin^[50] package in MATLAB.

X-ray Crystallography

Single crystals of complexes **1**, **2**, **3**, **1-NCMe**, **2-NCMe**, **3-NCMe**, **1-PF₆**, and **3-NCMePF₆** were obtained by vapor diffusion of diethyl ether into a concentrated acetonitrile solution of the appropriate complex. Single crystals of **4** were obtained by slow cooling a concentrated solution of the species in hexanes. Single crystals of **2-red** were obtained by vapor diffusion of pentane into a concentrated solution of the species in THF. Single crystals of **Bn₃daf** were obtained by vapor diffusion of pentane into a concentrated solution of the species in CHCl₃. Single-crystal X-ray diffraction data were collected with a Bruker Proteum diffractometer equipped with two CCD detectors (Apex II and Platinum 135) sharing a common MicroStar microfocus Cu rotating anode generator running at 45 mA and 60 kV (Cu K α = 1.54178 Å). CCDC 2038430, 2038431, 2038432, 2038433, 2038434, 2038435, 2038436, 2038437, 2038438, 2038439, and 2038440 contain the supplementary crystallographic data for this paper. These data can be obtained free of charge from The Cambridge Crystallographic Data Centre.

Electrochemistry

Electrochemical experiments were carried out in a nitrogen-filled glove box. Tetra(n-butylammonium) hexafluorophosphate (0.10 M; Sigma-Aldrich; electrochemical grade) in acetonitrile served as the supporting electrolyte. Measurements were made with a Gamry Reference 600 Plus Potentiostat/Galvanostat using a standard three-electrode configuration. The working electrode was the basal plane of highly oriented pyrolytic graphite (HOPG, GraphiteStore.com, Buffalo Grove, Ill.; surface area: 0.09 cm²), the counter electrode was a platinum wire (Kurt J. Lesker, Jefferson Hills, PA; 99.99%, 0.5 mm diameter), and a silver wire immersed in electrolyte served as a pseudo-reference electrode (CH Instruments). The reference was separated from the working solution by a Vycor frit (Bioanalytical Systems, Inc.). Ferrocene (Sigma Aldrich; twice-sublimed) was added to the electrolyte solution at the conclusion of each experiment (~1 mM); the midpoint potential of the ferrocenium/ferrocene couple (denoted as Fc⁺⁰) served as an external standard for comparison of the recorded potentials. Concentrations of analyte for cyclic voltammetry were typically 2 mM.

Acknowledgements

The authors thank Justin Douglas and Sarah Neuenswander for assistance with NMR and EPR spectroscopy. This work was supported by the US National Science Foundation through award OIA-1833087. W.C.H. was supported by the US National Institutes of Health Graduate Training Program in the Dynamic Aspects of Chemical Biology (T32 GM008545-25) as well as by a Graduate Student Research Grant from the Kansas Academy of Science. J.P.S. was supported by the Beckman Scholars Program at the University of Kansas, funded by the Arnold & Mabel Beckman Foundation. Support for NMR instrumentation was provided by the NIH (S10OD016360, S10RR024664) and NSF (CHE-1625923), and support for EPR instrumentation was provided by the NSF (CHE-0946883).

Conflicts of Interest

The authors declare no conflict of interest.

Keywords: ligands • redox chemistry • electrochemistry • rhodium • crystallography

References

- [1] a) T. R. O'Toole, L. D. Margerum, T. D. Westmoreland, W. J. Vining, R. W. Murray and T. J. Meyer, *J. Chem. Soc., Chem Commun.* **1985**, 1416-1417. b) B. P. Sullivan, C. M. Bolinger, D. Conrad, W. J. Vining and T. J. Meyer, *J. Chem. Soc., Chem Commun.* **1985**, 1414-1416. c) D. V. Yandulov and R. R. Schrock, *Science* **2003**, *301*, 76. d) J. S. Anderson, J. Rittle and J. C. Peters, *Nature* **2013**, *501*, 84.
- [2] a) U. Kölle, M. Grätzel, *Angew. Chem.* **1987**, *99*, 572-574; b) U. Kölle, M. Grätzel, *Angew. Chem. Int. Ed. Engl.* **1987**, *26*, 567-570.
- [3] a) M. Bourrez, F. Molton, S. Chardon-Noblat and A. Deronzier, *Angew. Chem. Int. Ed.* **2011**, *50*, 9903-9906. b) M. L. Clark, P. L. Cheung, M. Lessio, E. A. Carter and C. P. Kubiak, *ACS Catal.* **2018**, *8*, 2021-2029.

-
- [4] W. C. Henke, D. Lionetti, W. N. G. Moore, J. A. Hopkins, V. W. Day and J. D. Blakemore, *ChemSusChem* **2017**, *10*, 4589-4598.
- [5] (a) W. Kaim and B. Schwederski, *Coord. Chem. Rev.* **2010**, *254*, 1580-1588. (b) V. Lyaskovskyy and B. de Bruin, *ACS Catal.* **2012**, *2*, 270-279.
- [6] a) C. P. Anderson, D. J. Salmon, T. J. Meyer and R. C. Young, *J. Am. Chem. Soc.* **1977**, *99*, 1980-1982. b) G. F. Strouse, J. R. Schoonover, R. Duesing, S. Boyde, W. E. Jones, Jr., T. J. Meyer, *Inorg. Chem.* **1995**, *34*, 473-487. c) H. Takeda, K. Koike, H. Inoue and O. Ishitani, *J. Am. Chem. Soc.* **2008**, *130*, 2023-2031. d) H. Takeda, K. Koike, T. Morimoto, H. Inumaru and O. Ishitani in *Photochemistry and photocatalysis of rhenium(I) diimine complexes*, Vol. 63 Eds.: R. v. Eldik and G. Stochel), Academic Press, **2011**, pp. 137-186. e) J. England, C. C. Scarborough, T. Weyhermüller, S. Sproules and K. Wieghardt, *Eur. J. Inorg. Chem.* **2012**, *2012*, 4605-4621.
- [7] F. Blau, *Monatsh. Chem.* **1889**, *10*, 375-388.
- [8] C. Kaes, A. Katz and M. W. Hosseini, *Chem. Rev.* **2000**, *100*, 3553-3590.
- [9] J. Druey and P. Schmidt, *Helv. Chim. Acta* **1950**, *33*, 1080-1087.
- [10] L. J. Henderson, F. R. Fronczek and W. R. Cherry, *J. Am. Chem. Soc.* **1984**, *106*, 5876-5879.
- [11] V. T. Annibale, R. Batcup, T. Bai, S. J. Hughes and D. Song, *Organometallics* **2013**, *32*, 6511-6521.
- [12] a) H.-j. Pang, J.-q. Sha, J. Peng, A.-x. Tian, C.-j. Zhang, P.-p. Zhang, Y. Chen, M. Zhu and Y.-h. Wang, *Inorg. Chem. Commun.* **2009**, *12*, 735-738. b) H.-j. Pang, C.-j. Zhang, J. Peng, Y.-h. Wang, J.-q. Sha, A.-x. Tian, P.-p. Zhang, Y. Chen, M. Zhu and Z.-m. Su, *Eur. J. Inorg. Chem.* **2009**, *2009*, 5175-5180.
- [13] a) W. Wong, *Coord. Chem. Rev.*, **2005**, *249*, 971-997. b) K. Ono and K. Saito, *Heterocycles*, **2008**, *75*, 2381-2413. c) V. T. Annibale and D. Song, *Dalton Trans.*, **2016**, *45*, 32-49.
- [14] P. B. White, J. N. Jaworski, C. G. Fry, B. S. Dolinar, I. A. Guzei and S. S. Stahl, *J. Am. Chem. Soc.* **2016**, *138*, 4869-4880.
- [15] F. G. Bordwell, *Acc. Chem. Res.* **1988**, *21*, 456-463.
- [16] a) H. Jiang, E. Stepowska and D. Song, *Dalton Trans.* **2008**, 5879-5881. b) R. Tan, F. S. N. Chiu, A. Hadzovic and D. Song, *Organometallics* **2012**, *31*, 2184-2192. c) V. T. Annibale, R. Batcup, T. Bai, S. J. Hughes and D. Song, *Organometallics* **2013**, *32*, 6511-6521. d) R. Batcup, V. T. Annibale and D. Song, *Dalton Trans.* **2014**, *43*, 8951-8958. e) V. T. Annibale and D. Song, *Organometallics* **2014**, *33*, 2776-2783. f) T. Janes, K. M. Osten, A. Pantaleo, E. Yan, Y. Yang and D. Song, *ChemComm.* **2016**, *52*, 4148-4151. g) T. Janes, V. T. Annibale and D. Song, *J. Organomet. Chem.* **2018**, *872*, 79-86.
- [17] H. Jiang and D. Song, *Organometallics* **2008**, *27*, 3587-3592.
- [18] E. Stepowska, H. Jiang and D. Song, *ChemComm.* **2010**, *46*, 556-558.
- [19] H. Jiang, E. Stepowska and D. Song, *Eur. J. Inorg. Chem.* **2009**, *2009*, 2083-2089.
- [20] A. N. Campbell, P. B. White, I. A. Guzei and S. S. Stahl, *J. Am. Chem. Soc.* **2010**, *132*, 15116-15119.
- [21] a) T. Diao, T. J. Wadzinski and S. S. Stahl, *Chem. Sci.* **2012**, *3*, 887-891. b) W. Gao, Z. He, Y. Qian, J. Zhao and Y. Huang, *Chem. Sci.* **2012**, *3*, 883-886.
- [22] C. Creutz, *Comments Inorg. Chem.* **1982**, *1*, 293-311.
- [23] (a) W. Kaim, *Coord. Chem. Rev.* **1987**, *76*, 187-235. (b) W. Kaim, A. Klein and M. Glöckle, *Acc. Chem. Res.* **2000**, *33*, 755-763.
- [24] a) M. Ladwig and W. Kaim, *J. Organomet. Chem.* **1992**, *439*, 79-90. b) W. Kaim, R. Reinhardt, E. Waldhoer and J. Fiedler, *J. Organomet. Chem.* **1996**, *524*, 195-202.
- [25] a) J. O. Taylor, R. Culpeck, A. M. Chippindale, M. J. Calhorda and F. Hartl, *Organometallics* **2021**, *40*, 1598-1613. b) J. Tory, L. King, A. Maroulis, M. Haukka, M. J. Calhorda and F. Hartl, *Inorg. Chem.* **2014**, *53*, 1382-1396.

-
- [26] M. A. Scharwitz, I. Ott, Y. Geldmacher, R. Gust and W. S. Sheldrick, *J. Organomet. Chem.* **2008**, *693*, 2299-2309.
- [27] J. J. Soldevila-Barreda, A. Habtemariam, I. Romero-Canelón, and P.J. Sadler, *J. Inorg. Biochem.*, **2015**, *153*, 322-333.
- [28] E. Gore-Randall, M. Irwin, M. S. Denning, J. M. Goicoechea, *Inorg. Chem.* **2009**, *48*, 8304-8316.
- [29] The ligands themselves were prepared from 1,10-phenanthroline (phen), which is readily oxidized by manganate to produce dafone. Wolff-Kishner reduction of dafone generates daf, and sequential deprotonation of daf with potassium *tert*-butoxide (tBuOK) followed by addition of iodomethane affords access to Me₂daf.
- [30] H. Ohru, A. Senoo and T. Kosuge in *Preparation of diazafluorene compounds via palladium-catalyzed condensation reaction of diazafluorene dihalides with boronic acid derivatives*, Vol. Canon Kabushiki Kaisha, Japan. **2008**, p. 22.
- [31] Considering the straightforward synthesis of Me₂daf using iodomethane as an electrophile, we anticipated other electrophiles might be useful for generation of daf-type ligands. Unfortunately, use of benzyl bromide (BnBr) as an electrophile in this reaction sequence results in the apparent preferential formation of 9,9'-dibenzyl-1-N-benzyl-4,5-diazafluorenum bromide (**Bn₃daf**), an off-target compound that is confirmed using ¹H-NMR, mass spectrometry, and single crystal X-ray diffraction analysis (XRD, see Figures S24, S30, and S68). Thus, the use of BnBr here provides a contrasting result to what occurs when using iodomethane as the electrophile and was not pursued further.
- [32] A. Nutton, P. M. Bailey, P. M. Maitlis, *J. Chem. Soc. Dalton Trans.* **1981**, 1997-2002.
- [33] a) U. Kölle, M. Grätzel, *Angew. Chem.* **1987**, *99*, 572-574 ; b) U. Kölle, M. Grätzel, *Angew. Chem. Int. Ed. Engl.* **1987**, *26*, 567-570; *Angew. Chem.* **1987**, *99*, 572-574.
- [34] C. White, A. Yates, P. M. Maitlis and D. M. Heinekey, *Inorg. Synt.*, Vol. 29, Wiley- VCH, Weinheim, **1992**, 228-234.
- [35] M. A. Mantell, J. W. Kampf and M. Sanford, *Organometallics*, **2018**, *37*, 3240-3242.
- [36] W. C. Henke, J. A. Hopkins, M. L. Anderson, J. P. Stiel, V. W. Day, J. D. Blakemore, *Molecules* **2020**, *25*, 3189-3203.
- [37] The identity of the counteranion in the structures of the daf-type complexes was not found to significantly impact the structural properties of the [Cp*Rh] frameworks. In particular, the structure of **1** was compared here to the structure of [Cp*Rh(daf)Cl]PF₆ (denoted as **1-PF₆**; see SI, pp. S58-S61 and Table S2) and the structure of **3-NCMe** was compared to that of [Cp*Rh(Me₂daf)NCMe](PF₆)₂ (denoted as **3-NCMePF₆**; see SI, pp. S62-64 and Table S2). Considering this result, the structures of **1-NCMe**, **2-NCMe**, and **3-NCMe** can be compared to that of [Cp*Rh(bpy)NCMe](PF₆)₂ (**bpy^{NCMe}**), despite the presence of triflate counteranions in the solvento structures reported here.
- [38] M. A. Scharwitz, I. Ott, Y. Geldmacher, R. Gust and W. S. Sheldrick, *J. Organomet. Chem.* **2008**, *693*, 2299-2309.
- [39] J.D. Blakemore, E.S. Hernandez, W. Sattler, B.M. Hunter, L.M. Henling, B.S. Brunshwig, H.B. Gray, *Polyhedron*, **2014**, *84*, 14-18.
- [40] a) P. R. Sharp, D. W. Hoard and C. L. Barnes, *J. Am. Chem. Soc.*, **1990**, *112*, 2024-2026. b) D. W. Hoard and P. R. Sharp, *Inorg. Chem.*, **1993**, *32*, 612-620.
- [41] D. Lionetti, V. W. Day, B. Lassalle-Kaiser and J. D. Blakemore, *ChemComm.* **2018**, *54*, 1694-1697.
- [42] D. Lionetti, V. W. Day, J. D. Blakemore, *Dalton Trans.* **2019**, *48*, 12396-12406.
- [43] R. S. Nicholson and I. Shain, *Anal. Chem.* **1964**, *36* (4), 706-723.
- [44] M. K. Kalinowski, Z. R. Grabowski and B. Pakula, *T. Faraday Soc.* **1966**, *62*, 918-925.
- [45] Chemical reduction of **2-NCMe** using 1% Na(Hg) resulted in the generation of Na₂(4,5-diazafluorene)₂(4,5-diazafluorenyl)₂ (**2-red**), which was identified by X-ray crystallography (see SI, pp. S54-S55). This result

highlights the deleterious Brønsted acid-base reactivity that may occur without protective methylation of the doubly benzylic methylene protons of 4,5-diazafluorene.

- [46] J. A. Hopkins, D. Lionetti, V. W. Day and J. D. Blakemore, *Organometallics* **2019**, *38*, 1300-1310.
- [47] N. G. Connelly and W. E. Geiger, *Chem. Rev.* **1996**, *96*, 877-910.
- [48] W. N. G. Moore, W. C. Henke, D. Lionetti, V. W. Day and J. D. Blakemore, *Molecules* **2018**, *23*, 2857-2873.
- [49] Y. Peng, M. V. Ramos-Garcés, D. Lionetti and J. D. Blakemore, *Inorg. Chem.* **2017**, *56*, 10824-10831.
- [50] S. Stoll and A. Schweiger, *J. Magn. Reson.*, **2006**, *178*, 42-55.
- [51] D. Lionetti, V. W. Day and J. D. Blakemore, *Organometallics* **2017**, *36*, 1897-1905.
- [52] a) J. P. Maier and D. W. Turner, *Faraday Disc. Chem. Soc.* **1972**, *54*, 149-167. b) P. S. Braterman and J. I. Song, *J. Org. Chem.* **1991**, *56*, 4678-4682.
- [53] a) L. M. A. Quintana, S. I. Johnson, S. L. Corona, W. Villatoro, W. A. Goddard, M. K. Takase, D. G. VanderVelde, J. R. Winkler, H. B. Gray and J. D. Blakemore, *PNAS* **2016**, *113*, 6409-6414. b) C. L. Pitman, O. N. L. Finster and A. J. M. Miller, *ChemComm.*, **2016**, *52*, 9105-9108.
- [54] E. A. Boyd, D. Lionetti, W. C. Henke, V. W. Day and J. D. Blakemore, *Inorg. Chem.* **2019**, *58*, 3606-3615.
- [55] G. R. Fulmer, A. J. M. Miller, N. H. Sherden, H. E. Gottlieb, A. Nudelman, B. M. Stoltz, J. E. Bercaw, K. I. Goldberg, *Organometallics* **2010**, *29*, 2176-2179.
- [56] a) R. K. Harris, E. D. Becker, S. M. Cabral De Menezes, R. Goodfellow, P. Granger, *Pure Appl. Chem.* **2001**, *73*, 1795-1818; b) R. K. Harris, E. D. Becker, S. M. Cabral De Menezes, P. Granger, R. E. Hoffman, K. W. Zilm, *Pure Appl. Chem.* **2008**, *80*, 59-84.